Energy Transfer and Fabry-Perot Oscillation: A New Paradigm for Electrically Driven Laser in Quasi-2D Ruddlesden-Popper Perovskite Microplates Film

Krishna Bera (kberantunano@gmail.com)
Department of Physics, National Taiwan University
Chintam Hanmandlu
Center for Applied Sciences, Academia Sinica
Hung-I Lin
National Taiwan University https://orcid.org/0000-0001-9849-3138
Rapti Ghosh
Molecular-Science and Technology Program,Taiwan International Graduate Program, Academia Sinica
Vijay Kumar Gudelli
Department of Physics and Center for Theoretical Physics, National Taiwan University
Chao-Sung Lai
Department of Electronic Engineering, Chang Gung University
Chih-Wei Chu
Academia Sinica
Yang-Fang Chen
Department of Physics, National Taiwan University https://orcid.org/0000-0003-1203-5115

Article

Keywords: Metal-halide Perovskite, light-emitting diode, Fabry-Perot resonance, resonance energy transfer, electrically driven laser

Posted Date: December 13th, 2021

DOI: https://doi.org/10.21203/rs.3.rs-1121122/v1

Abstract

Recently emerged metal-halide hybrid perovskite (MHP) possesses superb optoelectronic features, which have great attention in solid-state lighting, photodetection, and photovoltaic applications. Because of its excellent external quantum efficiency, MHP acquires enormous potential for manifestation of ultra-low threshold optically pumped laser. However, demonstration of electrical-driven laser remains a challenge because of vulnerable degradation of perovskite, limited exciton binding energy, and intensity quenching and efficiency drop by non-radiative recombinations. In this work, we observed an ultralow-threshold (~ 18 $nJcm^{-2}$) optically pumped Fabry-Perot (F-P) laser from moisture insensitive mixed dimensional quasi-2D Rudlesden-Popper phase perovskite (RPP) microplates. Unprecedently, we demonstrated electrical-driven F-P laser with threshold ~ 0.15 Acm^{-2} from quasi-2D RPP by judicious combination of perovskite/hole transport layer (HTL) and electron transport layer (ETL) having suitable band alignment and thickness. Additionally, we showed tunibility of lasing modes by driving external electrical potential. Ultralow-threshold lasing is mainly ascribed by existence of F-P feedback resonance inside RPP microplate, and selective resonance energy transfer mechanism in-between microplates. Performing the finite difference time domain (FDTD) simulations, we confirmed the presence of F-P feedback resonance, and light trapping effect at perovskite/ETL contributing to laser action. Our discovery of electrical-driven laser from MHP opens an alternative avenue in developing optoelectronics.

1. Introduction

Versatile hybrid organic-inorganic MHP has drawn enormous attention in modern optoelectronics because of its large-scale and low-cost solution-processed synthesis, tailorable semiconducting behaviors, strong intrinsic light-matter interactions, and outstanding optoelectronic ownership. For example, balanced charge mobility (~ 24.0 $cm^2 V^{-1} s^{-1}$) with tunable direct bandgap, high photoluminescence quantum yield (~ 90%), large photon absorption coefficient (~ 4.0×10^4 cm^{-1}), small exciton binding energy, low charge trapping density (~ 10^{16} cm^{-3}), long exciton diffusion length and lifetime have been demonstrated.[1–4] These superb optoelectronic characteristic features endorsed its promising appliance in solar cells having high power conversion efficiency (~ 25%) which is comparable to the crystalline silicon (26%), ultrahigh and ultrafast photodetector (photoresponsivity ~ 10^8 AW^{-1} and response time ~ ns), solid-state light-emitting diode (LED) with high external quantum efficiency (EQE) ~ 21%, ultralow threshold optically pumped laser with lasing threshold ~ 220 $nJcm^{-1}$, and etc.[3, 5, 6] Recently perovskite LED (PeLED) has attracted an extensive attraction in solid-state lighting because of its high EQE and lower power consumption compared to conventional incandescent/fluorescence bulbs which comprise a minimum of 30% of total energy consumption.[7, 8] Such versatile PeLEDs have tremendous potential application compared with the traditional LEDs of III-V (GaAS & GaN), II-IV, and IV-VI (ZnS/CdSe QDs) semiconductor quantum dots fabricated by high-cost techniques, and opens a promising avenue in the reduction of energy consumption up to 75% for the lighting technology.[7, 8] Notably, the color of the emitted light of PeLEDs can be tuned by the well-known particle size quantum confinement effect.[9] In addition to their aforementioned performance in PeLEDs, the MHP also serves as an excellent gain

medium for optically pumped ultralow threshold laser, which represents its achievable foundation of prospective electrically driven laser. However, the demonstration of electrical pumped laser from PeLED device by using MHP as an active layer still remains a colossal challenge for the scientists in the field because of intrinsically vulnerable degradation of perovskite in oxygen and moisture, electric filed induced intensity quenching and efficiency droop, limited exciton binding energy, imbalance charge injection, and severe trap states assisted non-radiative recombinations because of poor quality film formation.[7, 10, 11] At high injection current density, these effects restrict the desirable brightness of PeLED and hinder its application in electrically pumped lasers.[7] Notably, the efficiency droop at high injected current density is caused by Joule heating due to Auger nonradiative recombination.[12] Besides, the phase segregation of MHP could destroy the color purity and stability.[13] In order to address the poor moisture stability challenge of MHP, recently, the layered perovskite or quasi 2D (two-dimensional) perovskite containing the organic spacers of phenylammonium or methylammonium group sandwiched in-between the inorganic octahedral lead halide blocks has been introduced.[2, 14] In these perovskite structures, the utilization of long-chain hydrophobic organic ligands diminishes the permeation of moisture inside the inorganic octahedrons, which impedes the decomposition of MHP from moisture.[2]

The developed adaptable semiconducting multi-layered quasi-2D Rudlesden-Popper phase perovskite (RPP) (the structural chemical formula is $A`A_{n-1}B_nX_{3n+1}$, where larger A` compared to A are organic ammonium cations intercalated between 2D RPP sheets, B is transition metallic cations, X is halide anions, and n represents the number of inorganic planes inside the 2D RPP with dimensionality) surfaced as auspicious material for PeLEDs with high EQE and optical gain medium for lasing operation.[8] In multiphase quasi-2D RPP perovskite, the energy bandgap gradually decreases as n value increases from 1 (corresponding to 2D) to ∞ (corresponding to 3D) because of the quantum confinement effect.[8] In a mixed dimensional quasi-2D RPP layered perovskite structure, the bandgap can be tuned by the number of inorganic sheets and multiple quantum wells are formed, where the inorganic sheets serve as wells and organic spacer layers act as barriers.[15, 16] Notably, the size of the quantum wells can be controlled through the variation of A` and A cations, which efficiently drives cascade energy transformation (funneling of charge carriers to the lower bandgap materials) and induces charge localization.[17] For widened size quantum well, the energy transformation becomes faster and efficient, which suppresses defect-induced Auger nonradioactive recombination and enhances the EQE of PeLED.[11, 17] As compared to their 3D counterparts of MHP, the quasi-2D RRP possesses high binding energy with improved excitons confinement, long diffusion length, smaller grain size, better epitaxial film morphology, and superior environmental stability under exposure of moisture and light.[8, 10, 11] Utilizing these superior properties of quasi-2D RPP, several ultralow threshold optically pumped lasers containing excellent whispering-gallery-mode (WGM) cavity with efficient optical feedback and adequate gain have been reported.[10, 18, 19] As an example, Li et al., demonstrated ultralow threshold lasing through efficient photon and exciton confinement in multiphase stacked RPP microplates having preferred orientation of organic ammonium (OA) cations.[10] However, the preferred orientation of insulation OA of this material limits charges transport, which reduces the radiative recombination and restricts its application in high EQE PeLED and

electrically pumped lasers. Recently, Lee et al., reported that the efficiency limitation of PeLED by using quasi-2D RPP can be overcome by utilizing randomly connected RP phases inside MHP instead of their preferred orientation, which can improve the charge conduction without hampering the photon and exciton confinement.[8] Several research efforts have been focused on the demonstration of high EQE PeLED by utilizing quasi-2D perovskite, however, their appliance in the demonstration of electrically driven lasing remains a dream of the researcher across the globe.

To dispatch previously mentioned challenges, we synthesized moisture insensitive randomly distributed mixed dimensional quasi-2D RP perovskite microplates through the incorporation of long-chain hydrophobic heptylammonium bromide inside lead bromide octahedrons. We observed the ultralow threshold optically pumped F-P lasing from the individual and disorder medium of tenacious luminescence quasi-2D RP perovskite microplates, which is much lower than all previous research reports. Spectacularly, we demonstrated electrically driven mode and color-tunable ultralow threshold laser from MHP by unique design and fabrication of light-emitting device through expedient consolidation of MHP/HTL and ETL.

2. Results And Discussion

2.1 Quasi-2D $(HA)_2(MA)_{n-1}Pb_nBr_{3n+1}$ RP Perovskite Synthesis, Structural, and Optical Properties

Strongly luminescent and highly stable mixed dimensionalities quasi 2D $(HA)_2(MA)_{n-1}Pb_nBr_{3n+1}$ RP perovskite contain randomly oriented stacked quantum well sheets, shown in Figure 1a, was synthesized by the solution-crystallization method through inserting the long-chain cation organic spacer of hydrophobic heptylammonium bromide (HABr = $C_7H_{15}NH_3Br$) between the $PbBr_3$ octahedron followed by the spin casting of stoichiometric precursors ($PbBr_2$, MABr, and HABr with MA/HA molar ratio 1:2) at room temperature. Synthesis detail of HABr precursor solution has been provided in the **Experimental** section. HABr has a large ionic radius which does not fit at the corner-sharing of lead halide octahedral 3D framework, and separates the 3D perovskite framework into layers.[20] The utilization of long-chain organic HABr, as shown in **Figure S1**, enhances moisture insensitivity through the aggregation of more hydrophobic heptylammonium cations in the upper surface of quasi-2D RP perovskite, which prevents moisture permeation and improves the material stability.[21] The hydrophobic behavior of our synthesized quasi-2D perovskite compared to bulk has been confirmed from contact angle measurement, as shown in **Figure S2**. Our synthesized quasi-2D perovskite contains the mixed dimension with different n values, which has been confirmed from multiple exciton peaks present in the measured photoluminescence (PL) and absorption spectra, as shown in Figure 1b and Figure 1c, respectively. This observation is consistent with several published reports on similar perovskites.[10, 17, 21] We achieve RP structure contains <n> = 1 - 6 with randomly oriented and connected mixed phase of quasi-2D ($1 \leq \langle n \rangle \leq 4$ with strong quantum confinement and $4 \leq \langle n \rangle \leq 6$ with weak quantum confinement), and 3D ($\langle n \rangle \geq 7$), which reveals a

phase transformation from higher-dimensional (3D) to lower-dimensional (2D) upon decreasing in <n>, as shown in Figure 1b, Figure 1c, and **Figure S3**. We estimated the photoluminescence quantum yield (PLQY) of quasi-2D RP phase perovskite ~ 69%, which is at least two times higher than the reported $(PEA)_2(CH_3NH_3)_{m-1}Pb_mBr_{3m+1}$ and $(OA)_2(MA)_{n-1}Pb_nBr_{3n+1}$ ordered RP phase perovskites.[8, 10] The randomly connected mixed dimensional RP-phase yields radiative recombination and adequate charge/energy transformation through the efficient coupling of different dimensions, which possesses wide variation of bandgap, and provides high PLQY and EQE in light-emission.[8, 10] Besides, the reduced grain size induces strong radiative recombination because of the quantum confinement effect, which increases the PLQY and EQE of light-emitting devices.[8] Increasing the average number of layers <n> that formed the mixed dimensional perovskite could also be used to enhance the stability through the improvement of hydrophobic behavior.[21] Since the average number of layers is equal to the number of $PbBr_6$ monolayer sheets inside the perovskite layer, as shown in Figure 1a, the binding energy and bandgap of quasi-2D perovskites are less than those of 2D perovskite (<n> = 1) and possess weaker quantum confinement with the enhancement of <n>.[22] The PL spectrum, shown in Figure 1b, measured under the illumination of 374 nm laser with laser power density ~ 11 $nJcm^{-2}$ shows one strong intensity peak located at ~ 522 nm in addition to multiple small intensity peaks at higher energies side. The peaks located at higher energies originate from the reduced dimensions (<n> = 2 - 6) of RP perovskite because of the quantum confinement.[10] Compared to pristine 2D perovskite, quasi-2D RP phase perovskite film contains high PLQY because of reduced nonradiative trappings. Notably, the nonradiative trappings suppress the optical gain,[10, 23] which is a major drawback for the creation of laser action. In order to investigate the origin of multiple peaks more precisely, we deconvoluted the PL spectrum, as shown in **Figure S3a**. The obtained multiple PL peak positions with a comparison of several published reports have tabulated in **Table S1**. Notably, the position of the PL peak is highly sensitive to the size of the perovskite microstructure because of particle size quantum confinement effects.[3] For further confirmation of multiple peaks from mixed dimensional RP phases in the PL spectrum, we investigated the absorption spectra of 2D, quasi-2D, and 3D perovskite films, as shown in Figure 1c and **Figure S3b**. Consistent with the PL spectrum, the lowest bandgap absorption located at ~ 519 nm in addition to several higher energies absorption peaks located at ~ 509 nm, 490 nm, 471 nm, 447 nm, 416 nm, and 400 nm were assigned to mixed dimensional RP phases with <n> = 7, 6, 5, 4, 3, 2, and 1, respectively. The absorption spectrum reveals a Stokes shift ~ 6 nm compared to the PL emission spectrum because of the well-known particle-size quantum confinement effect.[3, 24] This hybrid feature of quasi-2D perovskite films is also consistent with the previously published reports.[25, 26] The presence of multiple peaks observed in PL and absorption study has been further confirmed from X-ray diffraction (XRD) analysis, as shown in Figure 1d, and **Figure S4**. The XRD pattern discloses various diffraction peaks originated from randomly distributed mixed dimensional 2D and quasi-2D RP phases with <n> = 1 - 6. A detailed analysis of the XRD pattern has been provided in **Figure S4**. The inset of Figure 1d shows the schematic of randomly distributed mixed-dimensional perovskite phases. The random distribution of multiple perovskite phases confirmed from the intensity ratio of multiple peaks originated from different dimensions as observed in PL and absorption spectroscopy study. The obtained SEM (scanning electron microscope), and OM

(optical microscope) image, shown in Figure 1e, also support the spectroscopic observations. The perovskite layers with various sizes are stacked together to form large-sized irregular grain boundaries, as shown in Figure 1e. Finally, in order to confirm the origin of multiple PL and absorption peaks from randomly distributed different RP phases, we have estimated the bandgap of 3D, quasi 2D, and 2D perovskite materials from UV absorption and photoelectron emission spectra by utilizing the standard Tauc plot method, as shown in **Figure S4** and **Figure S5**. The films exhibited a similar bandgap with LUMO (lowest unoccupied molecular orbital) and HOMO (highest occupied molecular orbital). Based on our estimation of the bandgap, we draw a schematic of the energy-band diagram of mixed-phase RP perovskite, as shown in Figure 1f. It is evident that, as <n> increases, the bandgap is gradually reduced, and injected excitons can be funneled from higher bandgap to lower bandgap, which is advantageous for inducing strong radiative-recombination to enhance PLQY.[7, 8]

2.2 Optically Pumped Random and Fabry-Perot Laser from Quasi-2D RP Perovskite

In PL investigation, spectacularly, we demonstrated the random laser action from the disordered medium of randomly oriented multidimensional quasi-2d RP perovskite when the optical stimulation exceeds the lasing threshold for achieving population inversion. We measured the PL spectra under the variation of excitation energy density by utilizing a 374 nm pulse laser having pulse width and frequency 55ps and 40 MHz, respectively, as shown in Figure 2a. With the enhancement of optical pumped power density above the lasing threshold, the appearance of sharp random lasing peaks having average FWHM (full width at half-maximum) ~ 0.25 nm superimposed on broad spontaneous emission peak (FWHM ~ 20 nm) with abrupt intensity change has been observed, as shown in the Figure 2b. This investigation reveals the unyielding signature of the optically pumped random laser phenomenon, and the estimated lasing threshold is ~ 18 $nJcm^{-2}$. The estimated lasing threshold is much lower than the current reported 2D RP perovskites and other organic-inorganic hybrid organometallic compounds.[19, 27–29] The random lasing behavior was also further verified from the abrupt change in the exciton lifetime above lasing threshold in TRPL (time-resolved photoluminescence) and angle-dependent lasing spectra measurements, as shown in Figure 2c and **Figure S6**, respectively. Numerous facets behind the observation of the ultralow threshold in our synthesized RP perovskite have been discussed as follows. First, our RP phase perovskite exhibits robust PL with high optical gain. Second, multiple light scattering from randomly distributed ensembles of multidimensional RP phases, as shown in the SEM image of Figure 1e, provides efficient optical feedback to reduce the lasing threshold because of enormous light trapping in the disordered medium. More importantly, as shown in the OM image of Figure 1e, smooth surfaces of RP phase perovskite microplates can serve as F-P (Fabry-Perot) resonance cavities via excellent-quality of mirror reflections, which implement sufficient resonant feedback for producing ultralow threshold lasing. To investigate the F-P feedback mechanism from perovskite microplates, we measured the microplate-size (L) dependent lasing spectra, as shown in Figure 2d. This investigation affirms mode spacing ($\Delta\lambda$) of lasing spectra following the well-known F-P resonance formula, $\Delta\lambda = \frac{\lambda^2}{2nL}$, where n is the group refractive

index and λ is the emissive wavelength.[30] As shown in Figure 2d, it is evident that spacing of lasing spectra decreases, and a large number of lasing modes appear with the enhancement of the size of perovskite micro-crystal, which confirms the presence of F-P feedback mechanism in the origin of ultra-low threshold lasing spectra.[24] The presence of the F-P feedback mechanism has been further theoretically verified by finite difference time domain (FDTD) simulation. The simulation details have been provided in the numerical simulation (**NS**) section. The strong light scattering, and presence of optical resonance nodes (maximum field intensity) and antinodes (minimum field intensity) in the electrical field distribution profile for cubical and rectangular shapes of perovskite microcrystal, shown in Figure 2d and Figure 2f, respectively, reveal the strong light confinement for efficient feedback mechanism inside the perovskite microcrystal. The combined effect of multi-scattering induced coherent loops in the disordered multidimensional RP phase perovskite and F-P feedback inside the individual perovskite microplates produces a large optical gain and reduces the energy losses, which originates the ultralow threshold lasing.[24] The optical gain can also be enhanced by efficient photon confinement through suitable band alignment among different RP phases. In particular, nonradiative resonance energy transfer (RET) mediated by dipole-dipole interactions through the deep spectral overlapping in the emission and absorption bands of multidimensional RP phases, which can act as donor and acceptor, plays a very important role.[31−33] The RET process leads to the flow of the exciting energy throughout the ensemble of RP phases because of exciton migration. In our present investigation, we observed significant spectral overlap between the emission and absorption spectrum of different RP phases, shown in **Figure S7**, which is the necessary feature of RET process. For further clarification on the existence of RET process, we performed a time-resolved photoluminescence experiment to measure the exciton lifetime of donor and acceptor, as shown in **Figure S8**. This investigation reveals a faster decay of donor exciton lifetimes, yielding different transfer efficiencies, which is the conclusive signature of RET process. The RET efficiency greatly depends on excitation power-density because of the variation of local photonic-state density due to the simultaneous coexistence of spontaneous and stimulated emission.[33] As shown in Figure 2a, when excitation power-density reaches the lasing threshold, multiple lasing peaks from different dimensions of the RP phase due to stimulated emission are superimposed on the broad spontaneous emission peak. Further enhancement of excitation power density, laser output becomes stable due to sufficient energy transformation. The coherent energy transfer through the achievement of coherent photonic mode can provide high optical gain and ultralow threshold lasing. Furthermore, the RET process is beneficial to suppress the reabsorption effect in the film formed by microplates of similar size. All these outstanding features of optically pumped ultralow threshold lasing from RP phase perovskite guided us for its appliance in the electrically driven laser, which has high demands in the photonics industry from display to medical diagnosis.

Electroluminescence from Quasi-2D RP Perovskite and Energy Transfer

A light-emitting device was fabricated by combining our synthesized quasi-2D RP perovskite on top of an n-type ZnO (zinc oxide) ETL. Judiciously, an ultrathin HTL of PH1000 was used on top of the perovskite to supply sufficient carrier injection in light emission. The schematic of the fabricated device is shown in

Figure 3a. In order to fabricate the device, the bottom electrode gold (Au) was deposited on top of the Si/SiO_2 substrate by utilizing the thermal evaporation technique. The ETL ZnO having thickness ~ 220 nm was deposited on the Si/SiO_2/Au substrate by radio-frequency (RF) sputtering following the shadow mask method. RP perovskite film was fabricated on top of the previously fabricated device containing the ZnO layer by utilizing the solution-crystallization method. Then an ultrathin layer of PH100 having thickness ~ 20 nm was spin-coated on top of the perovskite. Finally, ITO (indium tin oxide) was used as the top electrode. Fabrication detail of the electroluminescence device has been supplied in **Experimental Section**. The corresponding SEM image of the fabricated device is shown in Figure 3b. I-V characteristic of the device shown in Figure 3c indicates the formation of the p-n junction of the device having an ideality factor ~ 1.8. The fabricated device has been optimized by subsequent measurements of turn-on voltage of the device from I-V curves through the variation of the thickness of perovskite and PH100. The estimated turn-on voltage of our fabricated device is ~ 1.0 V, which is well below the formerly reported LED devices based on RP-Phase perovskites.[34] Figure 3d shows the electroluminescence (EL) spectrum measured under the forward injection current density of 0.02 Acm^{-2}. Amusingly, the EL spectrum reveals the multiple emission peaks originated from different dimensionalities of quasi-2D RP perovskite consistent with the observed PL spectrum shown in Figure 1b. The EL emission peak originated from the higher dimensional 3D RP phase dominates over the emission peaks from lower dimensional RP phases because the smaller exciton confinement at the higher dimensional 3D RP phase possesses a lower bandgap. Intriguingly, with the enhancement of forward injection current densities, a progressive enhancement of EL peaks intensity originated from lower dimensionalities ($\langle n \rangle = 1 - 6$) as compared to 3D ($\langle n \rangle \geq 7$) RP phase has been observed, as shown in Figure 3e and Figure 3f. From the energy band diagram as shown in Figure 1f, it is evident that the high energy required for EL through charge accumulation in lower dimensionalities of the RP phase possesses a higher bandgap compared to 3D. At higher forward injection current, charge transformations through more carrier accumulations in lower dimensions of RP perovskite provide the dominating EL emissions. Besides, as discussed earlier, the possibility of the enhanced quantum confinement effect from 3D to lower dimensionalities can also provide strong light emission from quasi-2D perovskite compared to bulk.

2.3 Electrically Driven Laser from Quasi-2D RP Perovskite

Spectacularly, upon enhancement of forward injection current density, the broad EL emission peaks having average FWHM ~ 20 nm from different dimensionalities of RP perovskites evolved into the multiple narrow peaks containing average FWHM ~ 1.5 nm with robust enhancement of EL intensity, as shown in the Figure 4a. Attractively, EL emission peaks originated from 3D possess higher intensity as compared to other lower-dimensional emission peaks, as shown in Figure 4a. Inset shows the mobile photograph of the emitted green light from the device. Importantly, with further enhancement of the injection current above the lasing threshold, we observed the gradual suppression of higher dimensional EL emission peaks and the evolution of lower-dimensional EL peaks with a reduced FWHM down to ~ 0.8 nm, as shown in Figure 4b-f. We achieved strong blue lasing emission originated from lower dimensionalities corresponding to $\langle n \rangle = 2, 3$. The mobile photograph of the emitted strong blue lasing

light has been provided in the inset of Figure 4f. The variations of FWHM and light intensity with electrically pumping current density plot shown in Figure 5a reveal a sudden drop of FWHM and vigorous enhancement of EL intensity, which apparently acknowledges the electrical driven lasing action from quasi-2D RP perovskite having lasing threshold ~ 0.15 Acm^{-2}. The estimated lasing threshold is much lower than the previously reported electrical-driven semiconductor diode lasers.[35–37] As an example, Ra *et al.* reported a threshold current density ~ 400 Acm^{-2} in the electrically driven surface-emitting GaN semiconductor laser.[35] Suja *et al.* observed a random lasing threshold current ~ 20 mA in surface plasmon enhanced laser diode utilizing ZnO/Ag hetero-interface containing ZnO size ~ 700 nm × 50 μm.[36] Ellis *et al.* reported a lasing threshold current ~ 287 nA at 150 K temperature in GaAs quantum dot nanocavity laser having circular cavity diameter ~ 150 nm.[38] The multiple origins behind the observation of ultralow threshold electrical-driven laser action from quasi-2D RP perovskite have been interpreted as follows. First, as discussed earlier, strongly luminescent quasi-2D perovskite contains high optical PLQY and possesses smooth surface of microplate structure, which can serve as a F-P resonance cavity to provide excellent feedback resonance to produce high optical gain. In our fabricated lasing device, a judicious combination of crystalline quasi-2D perovskite microplate on the top high-quality ZnO film by RF sputtering can play the role of a F-P cavity as discussed in the optical measurement. Second, expedient choice of electron and hole transport layers having large carrier injection efficiency provides strong radiative-recombination, which can enhance the optical gain and cope optical loss. The overall output intensity and power of the emitted light grow linearly with forward injection current density, shown in Figure 5a and **Figure S9**, respectively, reveals the mitigation of Auger non-radiative recombination in our designed laser device architecture. Third, the possibility of light trapping effect in quasi-2D perovskite due to its higher refractive index (2.5) compared to ZnO (2.2) can provide the sharp narrowband low threshold lasing spectrum. In order to investigate the lasing mechanism by the light trapping effect in ZnO/perovskite heterostructure, we performed FDTD simulation for light extraction, as shown in Figure 5b, and **Figure S10**. Simulation details have been provided in the **NS** section. The electric field distributions obtained from FDTD simulation reveal distinct light confinement and scattering effects for different thicknesses of ZnO/perovskite heterostructure. From the FDTD simulation shown in Figure 5b, it is evident that excellent light trapping and scattering effects can be found. Interestingly, the electric field distribution profile of the FDTD simulation also reveals the possibility of strong light-scattering from the top and bottom part of ZnO/perovskite heterostructure, as shown in Figure 5b. Reflection of the emitted light from the gold can also modulate the scattered light, which can enhance the optical gain and reduce the lasing threshold. Fourth, quasi-2D perovskite possesses the ensembles of multi-dimensional phases with randomly distributed excitonic dipoles, as shown in Figure 5c. In low injection current density below the threshold, the random distribution of excitonic dipoles counteract the strong dipole-dipole coupling, which annihilates the domination of collective oscillation of such dipoles, and provides broad EL spectra from different dimensions of RP perovskite. The application of high injection current density above the threshold enhances the strong Columbic attractiveness of excitonic dipoles, which promotes the diploes coherence. Collective oscillation of such dipoles can trigger robust coherence phase synchronized narrow band lasing emission. The aforementioned investigations reveal that the strong ultralow threshold

electrically driven lasing action from quasi-2D RP perovskite are predominantly originated from the combined effect of the F-P feedback mechanism and RET mediated by dipole-dipole interactions. At high injection current density, the extremely strong blue lasing emission from the lower dimensionalities (<n> = 2, 3) of RP perovskite and suppression of EL emissions from other higher dimensionalities can be explained through the exciton lifetime and charge accumulation in addition to the population inversion mechanism. With an increment of forward injection current density, the gradual evolution of lower-dimensional lasing emission peaks and suppression of higher dimensional lasing peaks, shown in Figure 4, confirms the contribution of charge accumulation process in electrically driven lasing action. When applied injection current density increases, the rate of accumulation between LUMO-HOMO of lower dimensionalities is increased because of the enhanced recombination rate and the reduced exciton lifetime of charge carriers, which provides strong light irradiation from lower dimensionalities. The reduced exciton lifetime can be attributed to the increased quantum confinement effect. Additionally, because the density of states in the lower dimensional quasi-2D microplate is much less, the population inversion is easier to achieve, and the corresponding laser action can also occur easily. When the laser action is triggered, it enables to drastically enhances the recombination rate and reduces the exciton lifetime. Therefore, most of the injected charge carriers are transferred and accumulated into the lower dimensional microplates and the bright blue emission is dominated. The suppression and appearance of different lasing modes in our fabricated lasing device at different injection current-density indicate the tunability of lasing modes and colors by the externally driving potential, which can provide an additional feature to the optoelectronic industry. We verified the stability performance of our fabricated electrically driven RP perovskite light-emitting device through measurement of external quantum efficiency of green light emission over a long period of time more than two months, as shown in **Figure S11**. The long term stability of the device can be explained through several factors: (a) the moisture insensitive hydrophobic behavior of our synthesized perovskite material as discussed earlier, (b) optical and electrochemical stability of the perovskite lasing material having high quality factor, (c) excellent film formation due to utilization of RF-sputtering ZnO, and (d) outstanding passivation of ITO/HTL layers on the perovskite.

3. Conclusion And Perspective

Laser represents one of the greatest discoveries in human history for it possesses a tremendous application and penetrates into our daily life, spanning from optical communication, bio-imaging and surgery, to barcode scanning, and etc. Therefore, discovering a simple and cost-effective route to generate a laser system has always attracted intensive attention both in academic and industrial research. Nanomaterials are certainly one of the best class candidates for they get hold of many unique features, such as tunable physical properties and high emission efficiency. However, even though through a great effort for decades, electrically driven nanomaterial lasers still remain an unresolved issue. In this study, a new paradigm based on the integration of Forest resonance energy transfer, multiple scattering induced coherent loops, and Fabry-Perot resonance have been proposed to circumvent this challenging issue. In this physical mechanism, when a thin film is composed of the size distribution of nanomaterials, if one of the wavelengths of the emitted light fulfills the condition of multiple scattering induced coherent loops

and Fabry-Perot resonance, the formation of coherent feedback loops of the light wave will achieve a strong optical gain with an enhanced recombination rate and starts to accumulate the energy flow from the nearby nanomaterials through the Forest resonance energy transfer. Therefore, electrically driven laser action can be easily obtained. To illustrate our proposed mechanism, recently emerged metal-halide hybrid multidimensional quasi-2D perovskite has been chosen. Unprecedently, we demonstrated ultralow threshold optical and electrical driven laser action from this versatile perovskite. Interestingly, we demonstrated the electrical tunability of lasing modes and color through the evolution of strong lower-dimensional, and suppression of higher-dimensional lasing modes. Our breakthrough discovery of electrical-driven laser action from quasi-2D RP perovskite not only eradicates the decade challenge of utilization organic-inorganic hybrid perovskite in the lasing device, but also adds insight to the academic research with an alternative mechanism. The discovered approach can be implemented into many other material systems, which should be very useful and timely for the future development of optoelectronic industry and its appliance from communication to medical diagnosis.

4. Experimental Section:

4.1 Synthesis of $C_7H_{15}NH_3Br$ Precursor: The first 4 mL n-heptylamine was added to 40 mL methanol solvent in a 250 mL round bottom flask. Then 4 mL HBr aqueous solution (≥ 45 wt %) was dropwise added into the flask, and the mixture was strong stirring under N2 atmosphere. Then the mixture was stirred at room temperature for about two hours. Subsequently, a crude oil-like product was obtained after evaporating the solvent by a rotary evaporator at 50 °C. Then the product was washed with diethyl ether three times. After the recrystallization and filtration, the precipitated white product $C_7H_{15}NH_3Br$ was collected, then dried under a vacuum at 60 °C for overnight. The dried $C_7H_{15}NH_3Br$ powder was stored in a glove box.

4.2. Optically Pumped Lasing Device Fabrication: Optically pumped lasing devices were fabricated on SiO_2/Si substrate. First, the substrate was cleaned through subsequent ultrasonication with acetone and ethanol. Then synthesized quasi-2D RP perovskite obtained by the solution-crystallization method was put on the substrate by the subsequent spin casting of stoichiometric precursors. Finally, beautiful strongly luminescent quasi-2D perovskite microplates were obtained after the performing of annealing treatment at ~ 50 °C for 10 minutes.

4.3 Electrically Pumped Lasing Device Fabrication: In order to fabricate the electrically driven lasing device, an ultrasonically cleaned SiO_2/Si substrate has been used. The cleaned substrate was annealed to avoid unwanted contaminations. The different steps of the electrical lasing device fabrication have been provided in **Figure S12**. Under high vacuum conditions (<4 × 10^{-7} Torr), a gold layer on the top of the substrate was deposited by thermal evaporation, as shown in **Figure S12i** and **Figure S12ii**. The Au/SiO_2/Si was placed into magneto-sputtering system for deposition of n-type ZnO by following the shadow masking method, as shown in **Figure S12iii**. For performing sputtering, 99.9 % pure phase ceramic zinc contains cylindrical shape having diameter ~ 9 cm and 3-6 mm thickness was utilized as

the target. The target and substrate were separated by the distance ~ 14 cm. Sputtering was performed in the presence of mixed gas oxygen and argon under a high vacuum with pressure below ~ 10^{-5} Torr by using primary and diffusion pumps. After deposition of n-type ZnO, the active luminescence quasi-2D RP perovskite layer was deposited on the top of the ZnO layer by following the solution crystallization method and shadow masking technique, as shown in **Figure S12iv**. A thin HTL layer on the top of the perovskite was deposited by the spin coating method, as shown in **Figure S12v**. Finally, an ITO glass was put on the top of the device for electrical measurement, as shown in **Figure S12vi**.

Optical & Electronic Characterization: PL and lasing spectra were recorded from Horiba Jobin Yvon TRIAX 320 spectrometer associated with micro-photoluminescence setup having 600/mm and 1200 g/mm grating of spectral resolution 0.06 nm. Exciton lifetime was measured by TRPL from the same spectrometer detector by the excitation of 55 ps and 40 MHz pulsed laser. Electronic characterizations were performed by Keithley 2400 and Agilent B2912A electrometers. Absorption and photoelectron spectra were recorded by Jacob V-670 UV-Vis spectrometer. Electroluminescence spectra were measured Horiba Jobin Yvon iHR 550 spectrometer.

Numerical Simulation

The FDTD simulation was performed by commercial Lumerical electromagnetic software. In order to perform FDTD simulations for optical pumped lasing from perovskite, we consider microcrystal containing cubical and rectangular shapes having size d = 1.05 μm, emission center λ = 525 nm, and group refractive index ng = 2.4. Numerical modeling of electrical driven laser emission from perovskite/ZnO heterojunction was performed by three-dimensional FDTD method considering the random orientation of dipoles at the interface of the heterostructure. The electrical field distribution using FDTD simulation was performed for variation of heterojunction thickness from 0.5 μm to 2 μm considering the refractive index of perovskite and ZnO are 2.4 and 2.2, respectively.

Supporting Information

SI can be obtained from the Nature website.

Declarations

Author’s contribution

Prof. Y.F.C. & K.P.B. proposed the project. The project was supervised by prof. Y.F.C.. K.P.B. & C.H. contributed equally. C.H. and C.W.C. synthesized the quasi-2D perovskite material. K. P.B. designed & fabricated lasing devices, and measured all the optical and optoelectronic properties. H.L. performed FDTD simulation. K.P.B and Y.F.C wrote the manuscript.

Acknowledgments

The authors are acknowledging the Ministry of Science and Technology as well as Academia Sinica, Taiwan for supporting this work. Dr. Chih Wei Chu thanks the Ministry of Science and Technology (MOST) of Taiwan (107-2221-E-001-007-MY3).

References

1. Jeon, N.J. et al. Compositional engineering of perovskite materials for high-performance solar cells. *Nature* **517**, 476-480 (2015).

2. Lin, Y. et al. Unveiling the operation mechanism of layered perovskite solar cells. *Nat. Commun.* **10**, 1-11 (2019).

3. Bera, K.P. et al. Graphene Sandwich Stable Perovskite Quantum-Dot Light-Emissive Ultrasensitive and Ultrafast Broadband Vertical Phototransistors. *ACS Nano* **13**, 12540-12552 (2019).

4. Gunnarsson, W.B. & Rand, B.P. Electrically driven lasing in metal halide perovskites: Challenges and outlook. *APL Mater.* **8**, 030902 (2020).

5. Correa-Baena, J.-P. et al. Promises and challenges of perovskite solar cells. *Science* **358**, 739-744 (2017).

6. Zhu, H. et al. Lead halide perovskite nanowire lasers with low lasing thresholds and high quality factors. *Nat. Mater.* **14**, 636-642 (2015).

7. Tsai, H. et al. Stable Light-Emitting Diodes Using Phase-Pure Ruddlesden-Popper Layered Perovskites. *Adv. Mater.* **30**, 1704217 (2018).

8. Lee, H.D. et al. Efficient Ruddlesden-Popper Perovskite Light-Emitting Diodes with Randomly Oriented Nanocrystals. *Adv. Funct. Mater.* **29**, 1901225 (2019).

9. Shirasaki, Y., Supran, G.J., Bawendi, M.G. & Bulović, V. Emergence of colloidal quantum-dot light-emitting technologies. *Nat. Photonics* **7**, 13 (2013).

10. Li, M. et al. Enhanced exciton and photon confinement in Ruddlesden–Popper perovskite microplatelets for highly stable low-threshold polarized lasing. *Adv. Mater.* **30**, 1707235 (2018).

11. Sun, B., Xu, Y., Chen, Y. & Huang, W. Two-dimensional Ruddlesden-Popper layered perovskite for light-emitting diodes. *APL Mater.* **8**, 040901 (2020).

12. Nikoobakht, B. et al. High-brightness lasing at submicrometer enabled by droop-free fin light-emitting diodes (LEDs). *Sci. adv.* **6**, eaba4346 (2020).

13. Slotcavage, D., Karunadasa, H. & McGehee, M.

14. Stoumpos, C.C. et al. Ruddlesden-Popper hybrid lead iodide perovskite 2D homologous semiconductors. *Chem. Mater.* **28**, 2852-2867 (2016).

15. Wang, N. et al. Perovskite light-emitting diodes based on solution-processed self-organized multiple quantum wells. *Nat. Photon.* **10**, 699-704 (2016).

16. Proppe, A.H. et al. Photochemically cross-linked quantum well ligands for 2D/3D perovskite photovoltaics with improved photovoltage and stability. *J. Am. Chem. Soc.* **141**, 14180-14189 (2019).

17. Yuan, M. et al. Perovskite energy funnels for efficient light-emitting diodes. *Nat. Nanotechnol.* **11**, 872-877 (2016).

18. Zhang, Q., Ha, S.T., Liu, X., Sum, T.C. & Xiong, Q. Room-temperature near-infrared high-Q perovskite whispering-gallery planar nanolasers. *Nano Lett.* **14**, 5995-6001 (2014).

19. Raghavan, C.M. et al. Low-Threshold Lasing from 2D Homologous Organic-Inorganic Hybrid Ruddlesden-Popper Perovskite Single Crystals. *Nano Lett.* **18**, 3221-3228 (2018).

20. Cao, D.H., Stoumpos, C.C., Farha, O.K., Hupp, J.T. & Kanatzidis, M.G. 2D Homologous Perovskites as Light-Absorbing Materials for Solar Cell Applications. *J. Am. Chem. Soc.* **137**, 7843-7850 (2015).

21. Shao, Y. et al. Stable Graphene-Two-Dimensional Multiphase Perovskite Heterostructure Phototransistors with High Gain. *Nano Lett.* **17**, 7330-7338 (2017).

22. Hanmandlu, C., Singh, A., Boopathi, K.M., Lai, C.-S. & Chu, C.-W. Layered perovskite materials: key solutions for highly efficient and stable perovskite solar cells. *Rep. Prog. Phys.* **83**, 086502 (2020).

23. Chong, W.K. et al. Dominant factors limiting the optical gain in layered two-dimensional halide perovskite thin films. *Phys. Chem. Chem. Phys.* **18**, 14701-14708 (2016).

24. Bera, K.P. et al. Intrinsic Ultralow-Threshold Laser Action from Rationally Molecular Design of Metal-Organic Framework Materials. *ACS Appl. Mater. Interfaces* **12**, 36485-36495 (2020).

25. Wang, N. et al. Perovskite light-emitting diodes based on solution-processed self-organized multiple quantum wells. *Nat. Photon.* **10**, 699-704 (2016).

26. Yuan, M. et al. Perovskite energy funnels for efficient light-emitting diodes. *Nat. Nanotechnol.* **11**, 872-877 (2016).

27. Zhao, C. & Qin, C. Quasi-2D lead halide perovskite gain materials toward electrical pumping laser. *Nanophotonics* (2021).

28. Medishetty, R. et al. A New Class of Lasing Materials: Intrinsic Stimulated Emission from Nonlinear Optically Active Metal–Organic Frameworks. *Adv. Mater.* **29**, 1605637 (2017).

29. He, H. et al. Polarized three-photon-pumped laser in a single MOF microcrystal. *Nat. Commun.* **7**, 11087 (2016).

30. Xu, Z. et al. Low-threshold nanolasers based on slab-nanocrystals of H-aggregated organic semiconductors. *Adv. mater.* **24**, Op216-220 (2012).

31. Shadak Alee, K., Barik, S. & Mujumdar, S. Förster energy transfer induced random lasing at unconventional excitation wavelengths. *Appl. Phys. Lett.* **103**, 221112 (2013).

32. Shen, T.-L. et al. Coherent Förster resonance energy transfer: A new paradigm for electrically driven quantum dot random lasers. *Sci. adv.* **6**, eaba1705 (2020).

33. Shi, X., Tong, J., Liu, D. & Wang, Z. Resonance energy transfer process in nanogap-based dual-color random lasing. *Appl. Phys. Lett.* **110**, 171110 (2017).

34. Liu, X.-K. & Gao, F. Organic-inorganic hybrid ruddlesden-popper perovskites: an emerging paradigm for high-performance light-emitting diodes. *J. Phys. Chem. Lett.* **9**, 2251-2258 (2018).

35. Ra, Y.-H. et al. An electrically pumped surface-emitting semiconductor green laser. *Sci. Adv.* **6**, eaav7523 (2020).

36. Suja, M. et al. Electrically driven plasmon-exciton coupled random lasing in ZnO metal-semiconductor-metal devices. *Appl. Surf. Sci.* **439**, 525-532 (2018).

37. Lu, Y.-J. et al. Plasmonic nanolaser using epitaxially grown silver film. *science* **337**, 450-453 (2012).

38. Ellis, B. et al. Ultralow-threshold electrically pumped quantum-dot photonic-crystal nanocavity laser. *Nat. Photon.* **5**, 297-300 (2011).

Figures

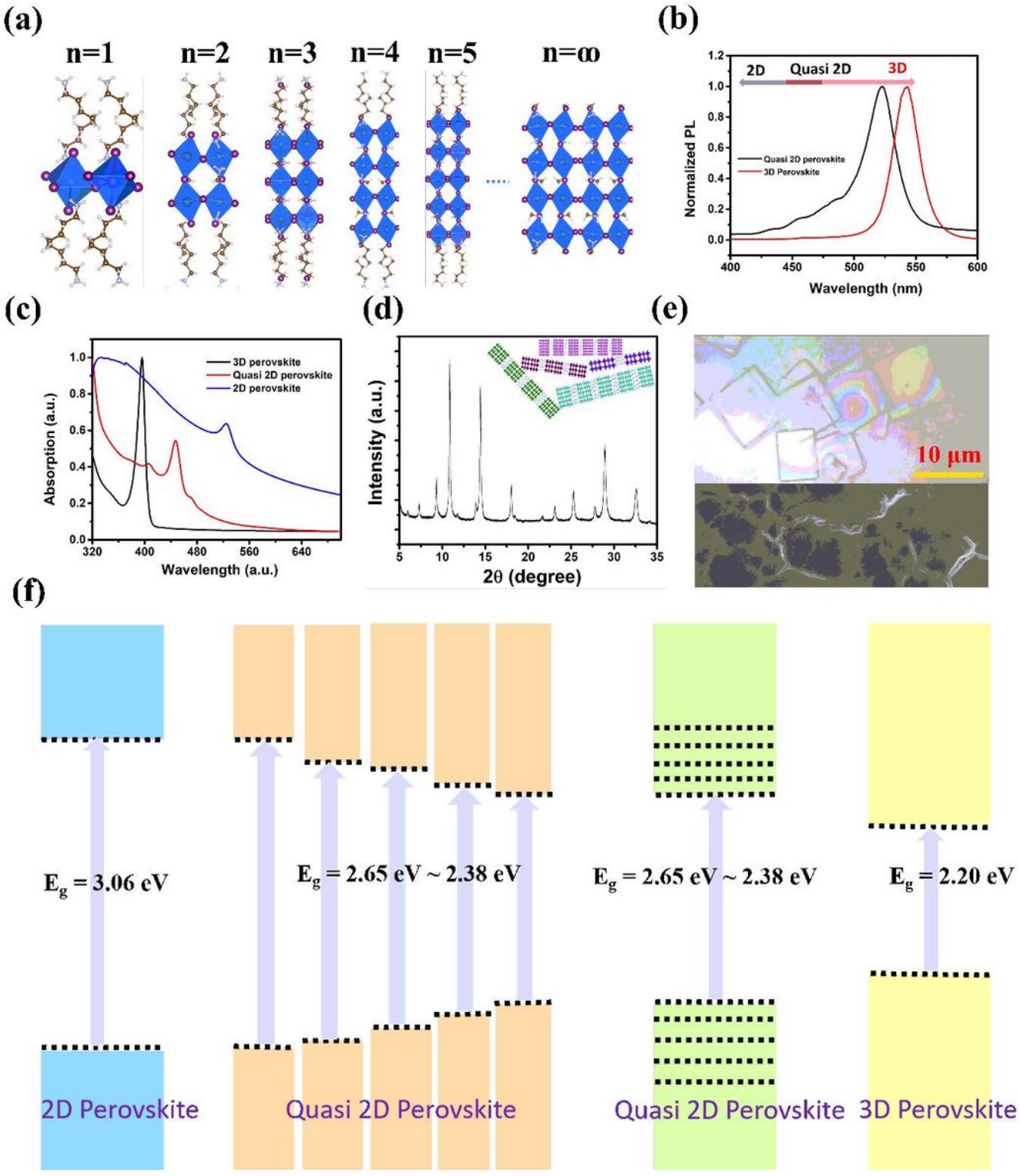

Figure 1

(a) Schematic of unit cell structure of (HA)2(MA)n-1PbnBr3n+1 RP perovskite with different n values, showing the evolution of dimensionality from 2D (n=1) to 3D (n = ∞). (b) PL spectra of quasi-2D and 3D perovskite films. (c) UV-visible absorption spectra of 2D, quasi-2D, and 3D perovskite films. (d) XRD patterns of quasi-2D perovskite film contain multiple peaks from different dimensions. Inset: schematic of different 'n' values of perovskites. (e) OM image of RPP perovskite microplates. Inset shows the SEM

image of the irregular grain boundaries formed by multiple stacked perovskite layers from different n. (f) Schematic of the energy-band diagram of mixed-phase RP perovskite based on estimation of the bandgap of 2D, quasi 2D, and 3D perovskite.

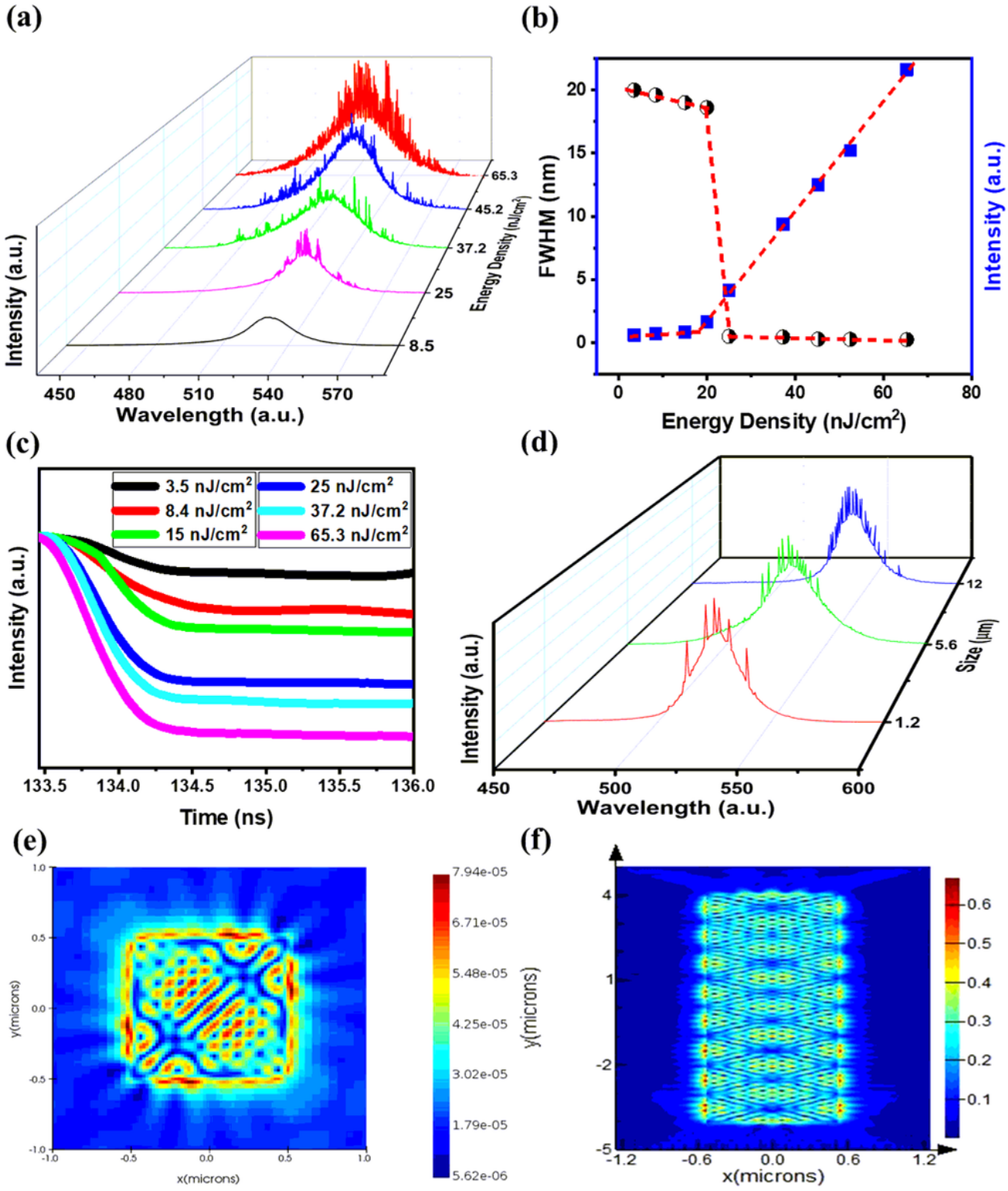

Figure 2

Lasing behavior of quasi-2D RP perovskite. (a) Optical energy-dependent lasing spectra. (b) Lasing threshold estimation from optical pumping-energy dependent FWHM and intensity of lasing spectra. (c)

Pumping-energy density-dependent TRPL curves below and above lasing threshold. (d) Size-dependent lasing spectra of quasi-2D perovskite under excitation fluence 30 nJcm-2. Mode spacing of lasing spectra decreases with the increase of size as an inverse relation. It confirms the presence of F-P cavity modes inside the perovskite microcrystal. (e) and (f) show the electrical field distribution profile obtained from FDTD simulation for considering cubical and rectangular shapes, respectively.

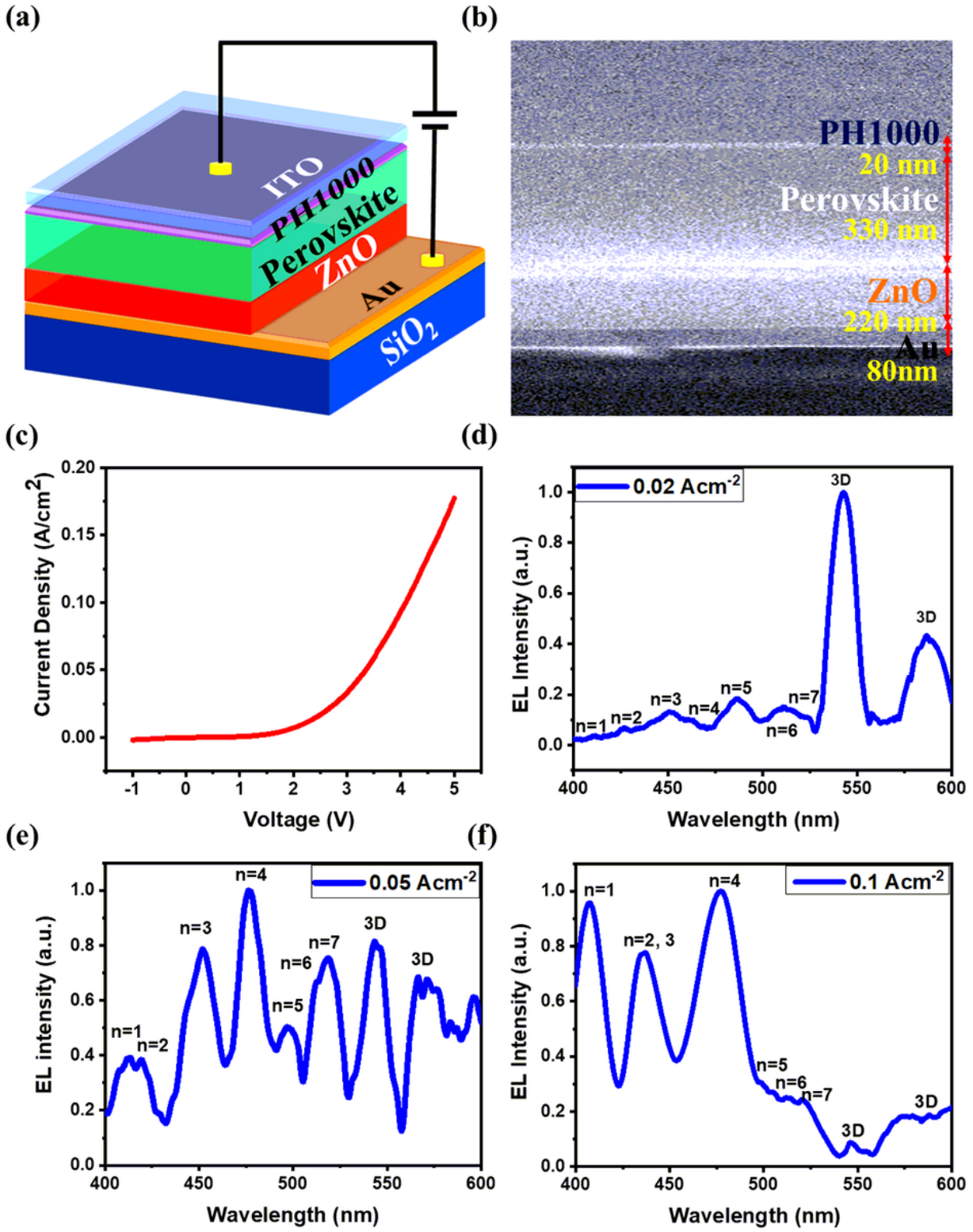

Figure 3

Electroluminescence from quasi-2D perovskite. (a) Schematic of electroluminescence device. (b) Corresponding SEM image of the fabricated device. (c) I-V characteristic of the EL device. (d), (e), and (f) are the EL spectra of device at different forward injection currents of 0.02 Acm-2, 0.05 Acm-2, and 0.1 Acm-2, respectively.

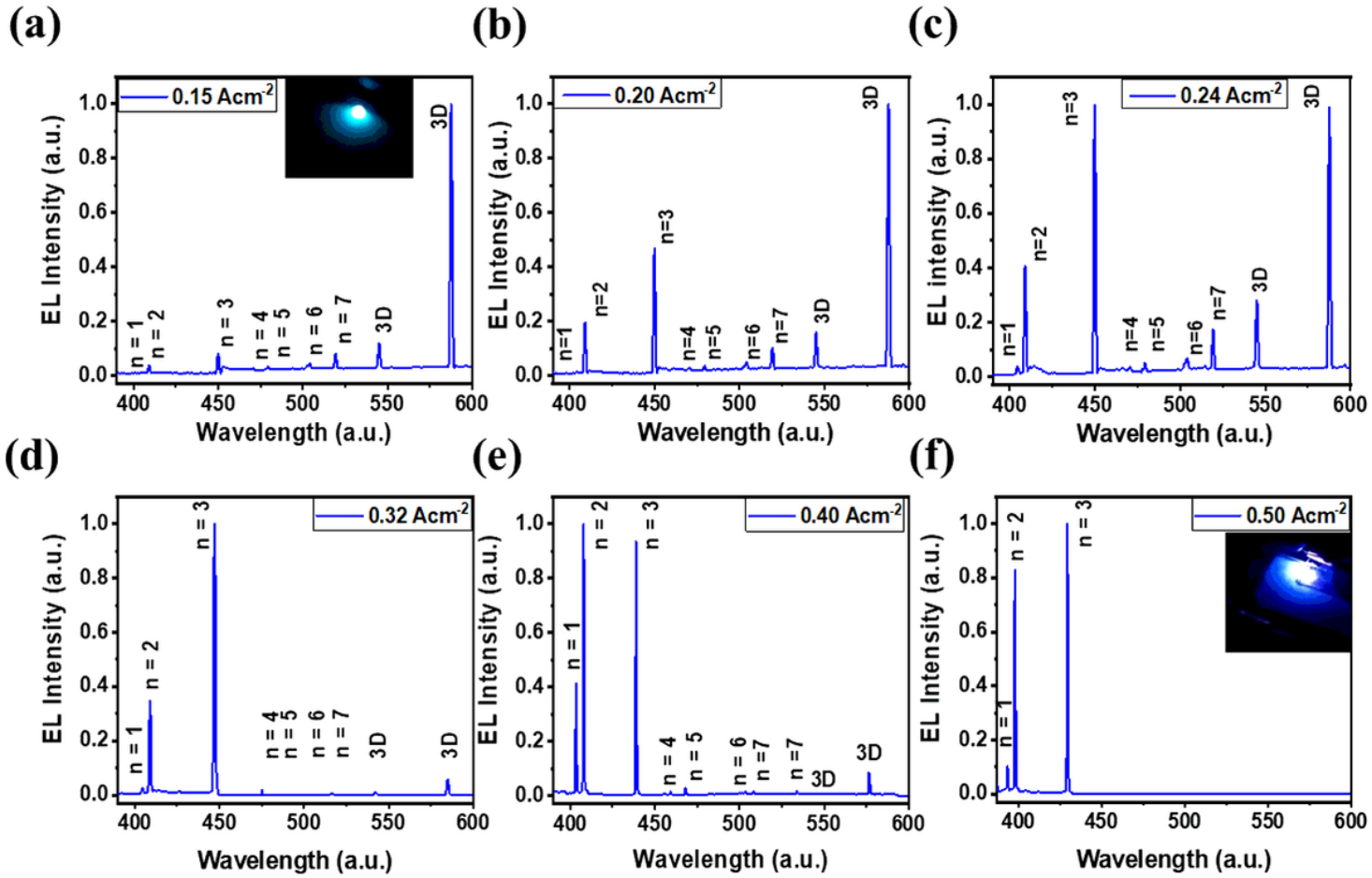

Figure 4

Electrically driven laser, and tunability of lasing modes and color. (a), (b), (c), (d), (e), and (f) are EL spectra at various forward injection current densities above the lasing threshold. The suppression and evolution of lasing modes by driving electric field reveal the possibility of lasing mode tunability. The inset of (a) and (f) shows the mobile photograph of emitted green and blue light at a forward injection current density 0.15 Acm-2 and 0.5 Acm-2, respectively.

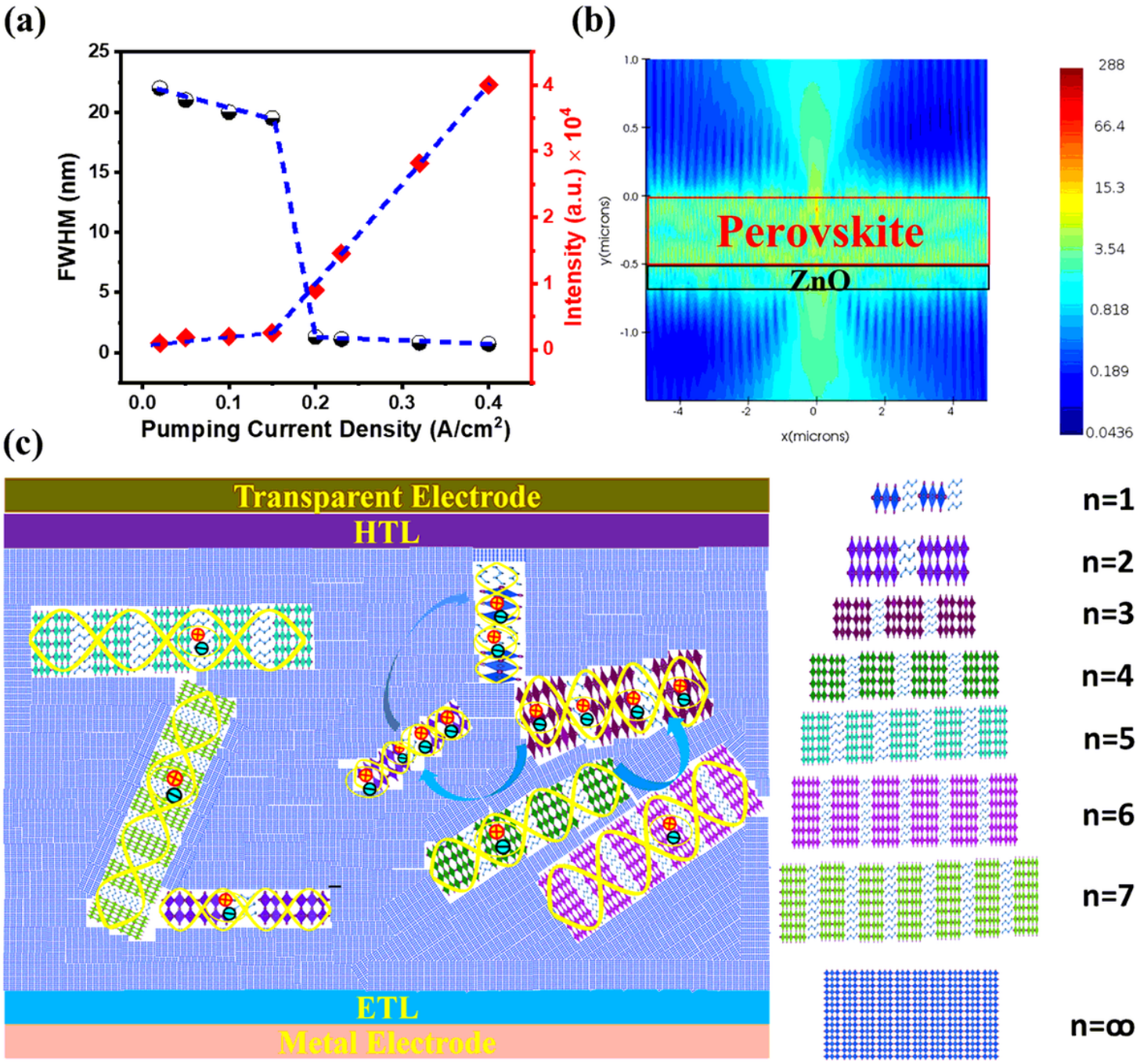

Figure 5

(a) Variation of EL intensity and FWHM with electrical pumping current density. (b) Light extraction profile of perovskite/ZnO heterostructure obtained from FDTD simulation considering the perovskite thickness. (c) Device structure with a schematic representation of proposed mechanism for multi modes laser-light emission through F-P and RET from the ensemble of randomly distributed excitonic dipoles in multi-dimensional quasi-2D perovskite.

Supplementary Files

This is a list of supplementary files associated with this preprint. Click to download.

- SUPPORTINGINFORMATION1.docx